

Introduction

The Swarm SCARF (Satellite Constellation Application and Research Facility), a consortium of several research institutions, has been established with the goal of deriving Level-2 products by combination of data from the three Swarm spacecraft. Here we present the results of the Swarm SCARF team at DTU Space and NASA Goddard who conducts the Comprehensive Inversion (CI) magnetic field model processing chain; we present the results from using five years of Swarm data denoted CIY5. The CI chain takes full advantage of the Swarm constellation by doing a comprehensive co-estimation of the magnetic fields from Earth's core, lithosphere, ionosphere, and magnetosphere together with induced fields from Earth's mantle and oceans using single and dual satellite gradient information. Level-2 products containing the corresponding model parameter estimations will be generated regularly and distributed via ESA at <http://swarm-diss.esa.int/Level2longterm/> (see <https://earth.esa.int/swarm> on how to gain access).

Model Parametrization, Data, and Data Selection

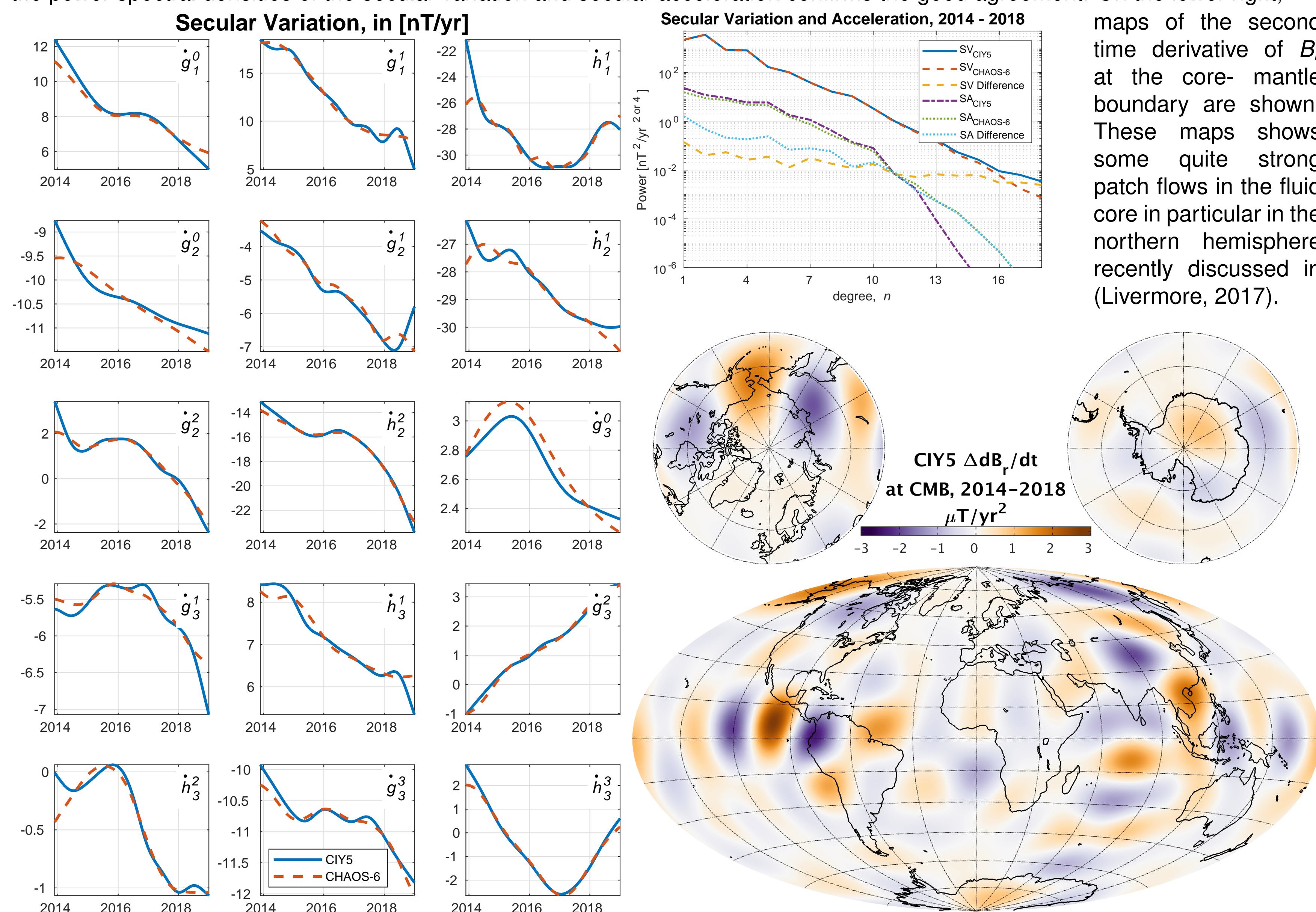
Table : Comprehensive Model Parametrization

Field	Description	Number of coefficients
Core	Spherical harmonic expansion $n_{max} = 18$. Secular variation (SV) through order 5 B-splines with $\frac{1}{2}$ year knot spacing, damping of 2 nd and 3 rd derivative of B_r .	5,040
Lithosphere	Spherical harmonic expansion $n = 19 \dots 120$	14,280
Ionosphere	Spherical harmonic expansion in quasi-dipole (QD) frame, underlying dipole SH $n_{max} = 60$, $m_{max} = 12$. Temporal: annual, semi-annual, 24-, 12-, 8- and 6-hr periodicities with F10.7 scaling plus induction via a-priori 3-D conductivity model ("1-D+oceans") and infinite conductor at core-mantle boundary (CMB)	5,520
Magnetosphere	Quiet times: Spherical harmonic expansion $n_{max} = 1$ external and internal (induced). Discretized in 1 hour bins. All data: $n_{max} = 2$, $m_{max} = 1$ external, $n_{max} = m_{max} = 3$ internal; dipole terms in $\frac{1}{2}$ hour bins, other terms in 6 hour bins.	368,364 or 216,108
M ₂ Tidal	Spherical harmonic expansion $n_{max} = 18$. Periodicity: 12.42060122 hr, phase fixed with respect to 00:00:00, 1999 January 1 GMT.	740
Nuisance	Day-side core, lithosphere, and M ₂ tidal, ground observatory biases, spacecraft alignment	22,675
Total		416,619

Swarm satellite data for this work consist of magnetic field measurements version 0505/06 from the period 25 November 2013 through 2018 with gross outliers removed and decimated to 30 second sampling rate; along-track differences ("gradients") are formed by taking single satellite differences separated by 15 seconds, whereas cross-track differences are formed from the lower Swarm pair, Alpha and Charlie, taking measurements at equal geographical latitude temporally separated by typically 4 to 15 seconds. The optimum satellite constellation for the cross-track differences was obtained and maintained since mid April 2014. Available hourly mean values from 163 ground based magnetic observatories for the period 25 November 2013 through October 2018 have been included in the modelling. Magnetically quiet periods were selected for the modelling – except for the modelling of the continuous magnetospheric field – based on Kp and Dst such that $Kp \leq 2^-$ for direct measurements and $Kp \leq 3^0$ for differences, and commonly $|\frac{dDst}{dt}| \leq 3nT/hr$. Core and tidal fields are determined from night-side data only, i.e. with Sun at least 10° below the horizon.

Core Field and Secular Variation: Level 2 Product MCO SHA 2C

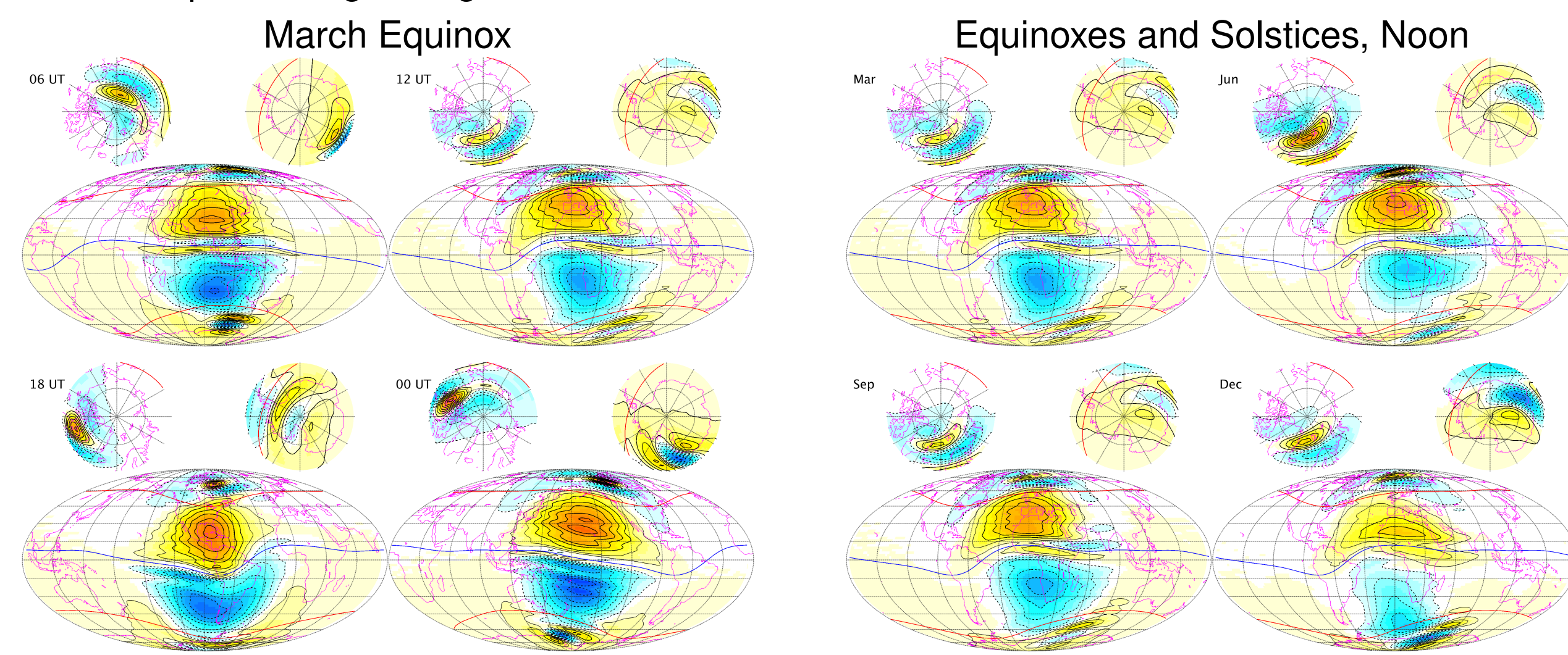
The core field estimated by the Comprehensive Inversion corresponds well with the CHAOS-6 model (Finlay, 2016) version x8 as can be seen from the plots of the first time derivatives of the Gauss coefficients ("Secular Variation") below on the left. In the middle, the power spectral densities of the secular variation and secular acceleration confirms the good agreement. On the lower right,



maps of the second time derivative of B_r at the core-mantle boundary are shown. These maps shows some quite strong patch flows in the fluid core in particular in the northern hemisphere recently discussed in (Livermore, 2017).

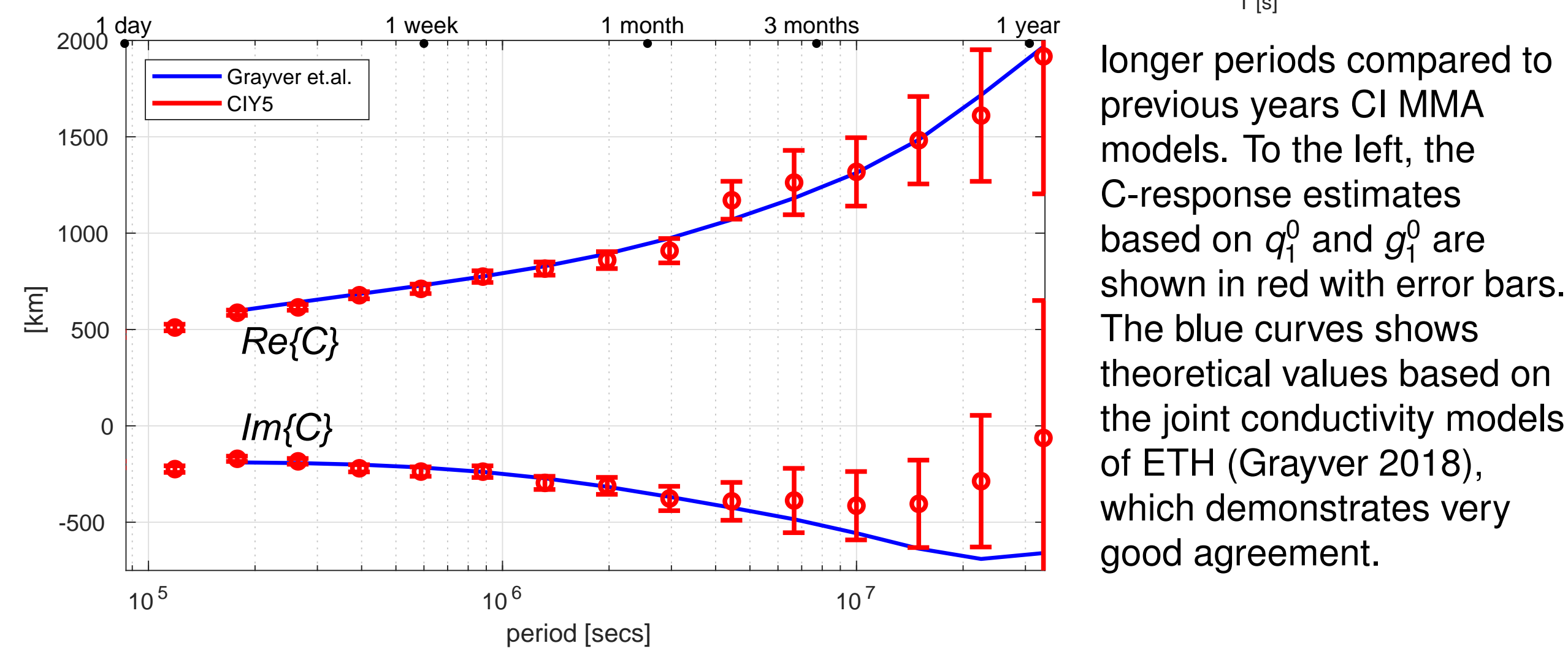
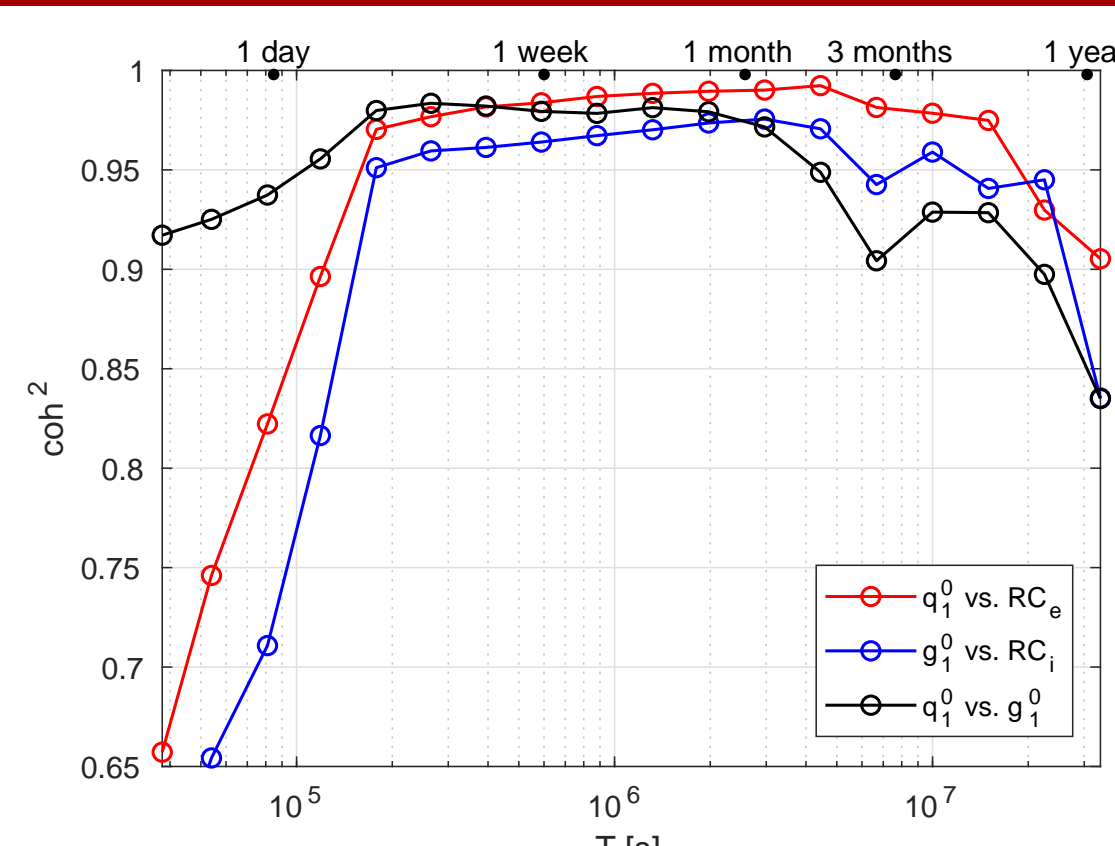
Ionospheric Field: Level 2 Product MIO SHA 2C

The figures below show the equivalent current function of the primary ionospheric currents for four different local times at the March equinox (left) and for four different epochs at noon (right). The dip equator is shown in blue, and the $\pm 55^\circ$ quasi dipole latitudes are shown in red. These maps are in good agreement with other models.



Magnetospheric Field: Level 2 Product MMA SHA 2C

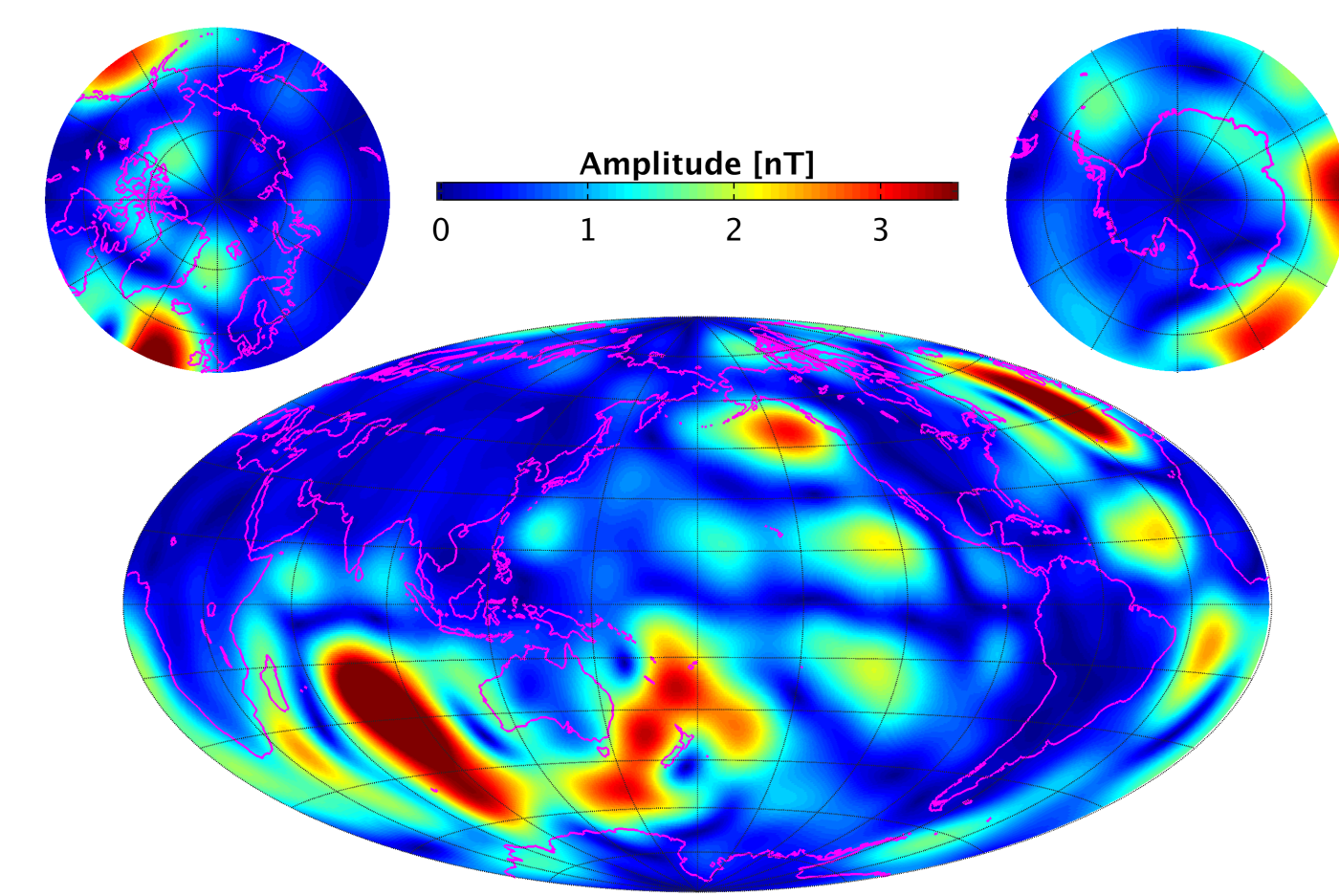
The magnetospheric field is estimated in two steps: First, data from magnetically quiet periods are used to estimate the models described above together with a preliminary magnetospheric model (the "Quiet times" model). Second, all data are used to estimate the "All data" model which is the official magnetospheric model of the CI chain. To the right, the squared coherences between q_1^0 and RC_e , g_1^0 and RC_i , and q_1^0 and g_1^0 are shown. This shows the continued increase in coherence for the



longer periods compared to previous years CI MMA models. To the left, the C-response estimates based on q_1^0 and g_1^0 are shown in red with error bars. The blue curves shows theoretical values based on the joint conductivity models of ETH (Grayver 2018), which demonstrates very good agreement.

Lunar M₂ Tidal Field: Level 2 Product MTI SHA 2C

On the plot to the left is shown the amplitude of the radial magnetic field induced by the Lunar M₂ tides at 400 km altitude. This shows the nice separation between land and sea as well as the main ocean tides.



Data Residual Statistics

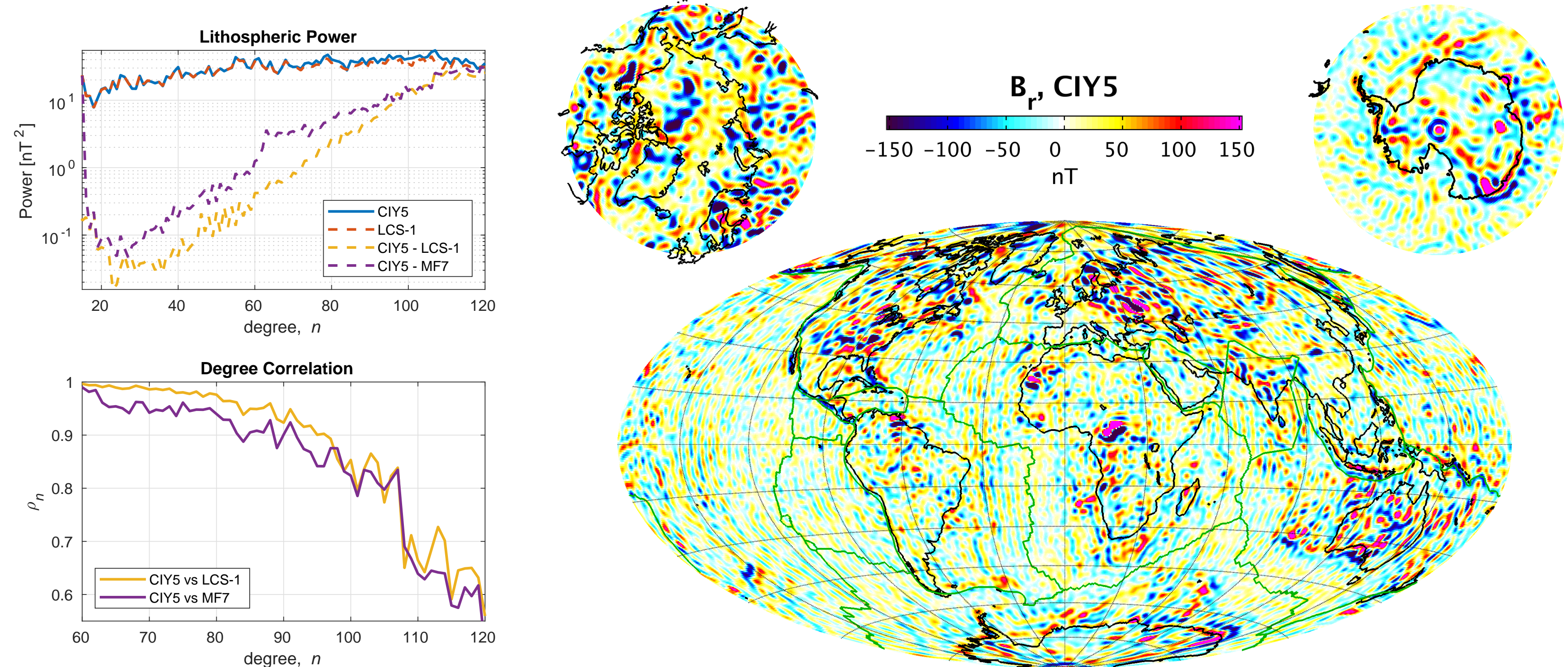
The residual statistics of the quiet time data vs. the comprehensive model (with "Quiet time" magnetospheric model) are listed in the table below. Grey cells indicate data from night-side, white cells indicate data from day-side (sunlit) periods. "Field" indicate the pure vector and scalar measurements, whereas "NS diff" and "EW diff" indicate the North-South (along-track) and East-West differences respectively. The standard deviations are quite impressive, and also show the almost perfect identity of the side-by-side flying pair Alpha and Charlie and in the North-South differences for all satellites. Swarm Bravo shows slightly higher residuals in most "Field" elements at low and mid latitudes though lower at high latitudes.

Table : Comprehensive Model Data Statistics

Sat	Geomagnetic Quasi Dipole (QD) Latitude, λ	Weighted Standard Deviation in nT								
		Low, $ \lambda \leq 10^\circ$		Mid, $ \lambda \in [10^\circ \dots 55^\circ]$		High, $ \lambda > 55^\circ$		$\sigma(F)$		
		$\sigma(B_r)$	$\sigma(B_\theta)$	$\sigma(B_r)$	$\sigma(B_\theta)$	$\sigma(B_r)$	$\sigma(B_\theta)$			
A	Field	1.63	1.92	1.66	2.41	1.65	2.09	2.07	1.78	5.62
	NS	0.31	0.18	0.32	0.16	0.24	0.28	0.35	0.18	0.93
	diff	0.89	0.76	0.79	0.68	0.49	0.53	0.82	0.31	1.05
B	Field	1.64	2.49	1.98	3.29	1.88	2.55	2.26	2.33	5.44
	NS	0.30	0.18	0.30	0.16	0.24	0.28	0.34	0.19	0.83
	diff	0.80	0.67	0.72	0.60	0.47	0.52	0.80	0.19	0.95
C	Field	1.64	1.87	1.64	2.38	1.65	2.08	2.07	1.78	5.62
	NS	0.32	0.18	0.32	0.16	0.25	0.29	0.35	0.18	0.93
	diff	0.90	0.76	0.78	0.68	0.49	0.54	0.82	0.31	1.05
A-C	EW	0.55	0.40	0.74	0.36	0.38	0.44	0.75	0.32	0.55
	diff	1.22	0.63	1.79	0.51	0.70	0.75	1.50	0.44	0.59

Lithospheric Field: Level 2 Product MLI SHA 2C

The part of the lithospheric field of degree $n \geq 19$ is determined solely from along-track (North-South) and cross-track (East-West) differences. Vector gradient information is used at low latitudes (QD-latitude below 55°) whereas scalar gradients are used at all latitudes. Both day- and night-side gradient information is used. We obtain excellent agreement between our model and the LCS-1 (Olsen, 2016), and MF7 (Maus, 2010) models with degree correlation above 0.8 up to spherical harmonic degree 105.



Conclusion

The results from the Comprehensive Inversion chain of the Swarm SCARF consortium applied to five years of Swarm data are very satisfactory. Using Swarm data together with magnetic observatories at ground we are able to estimate models of the internal and external magnetic fields of the Earth separated into models of the core, lithospheric, ionospheric, magnetospheric, and oceanic induced fields. These models agree very well with other magnetic field models estimated from Swarm and/or other data.

References

Finlay, C. C., et al., Recent geomagnetic secular variation from Swarm and ground observatories as estimated in the CHAOS-6 geomagnetic field model, *Earth, Planets and Space*, 68, 112 (DOI: 10.1186/s40623-016-0486-1), 2016.
 Friis-Christensen, E., et al., Swarm: A constellation to study the Earth's magnetic field, *Earth, Planets and Space*, 58, 351-358, 2006.
 Grayver, A., et al., Joint inversion of satellite-detected tidal and magnetospheric signals constrains electrical conductivity and water content of the upper mantle and transition zone, *Geophysical Research Letters*, 44(12), 6074-6081, (DOI: 10.1002/2017GL073446), 2017.
 Friis-Christensen, E., et al., Swarm: A constellation to study the Earth's magnetic field, *Earth, Planets and Space*, 58, 351-358, 2006.
 Grayver, A., et al., Joint inversion of satellite-detected tidal and magnetospheric signals constrains electrical conductivity and water content of the upper mantle and transition zone, *Geophysical Research Letters*, 44(12), 6074-6081, (DOI: 10.1002/2017GL073446), 2017.
 Livermore, P.W., et al., An accelerating high-latitude jet in Earth's core, *Nature Geoscience*, 10, 62-68 (DOI: 10.1038/ngeo2859), 2017.
 Maus, S., Magnetic field model MF7, *G3*, 2010.
 Olsen, N. et al., LCS-1: A high-resolution global model of the lithospheric magnetic field derived from CHAMP and Swarm satellite observations, *Geophysical Research Letters* (ISSN: 0094-8276) (DOI: 10.1002/2016GL068180), 2016.
 Sabaka, T. J. et al., A Comprehensive Model of Earth's Magnetic Field Determined From 4 Years of Swarm Satellite Observation, *Earth, Planets and Space* vol: 70, issue: 1 (DOI: 10.1186/s40623-018-0896-3) 2018.